Am J Cancer Res 2023;13(1):216-226
www.ajcr.us /ISSN:2156-6976/ajcr0145561

Original Article

Iron oxide nanoparticles inhibit tumor growth by ferroptosis in diffuse large B-cell lymphoma

Qi-Tang Huang[1*], Quan-Quan Hu[1,2*], Zhao-Feng Wen[1], Yan-Li Li[1,3]

[1]Department of Pathology, School of Basic Medical Sciences, Anhui Medical University, Hefei 230032, Anhui, China; [2]Department of Pathology, The Affiliated Anqing Hospital of Anhui Medical University, Anqing 246003, Anhui, China; [3]Department of Pathology, The Second Affiliated Hospital of Anhui Medical University, Hefei 230601, Anhui, China. [*]Equal contributors.

Received July 25, 2022; Accepted October 26, 2022; Epub January 15, 2023; Published January 30, 2023

Abstract: Since the approval by the Food and Drug Administration (FDA), ferumoxytol and other iron oxide nanoparticles (IONs) have been widely used as iron supplements for patients with iron deficiency. Meanwhile, IONs have also been used as contrast agents in magnetic resonance imaging and as drug carriers. Importantly, IONs have demonstrated a significant inhibitory effect on the growth of tumors, including hematopoietic and lymphoid tumors, such as leukemia. In this study, we further demonstrated the effect of IONs on inhibiting the growth of diffuse large B-cell lymphoma (DLBCL) cells by enhancing ferroptosis-mediated cell death. IONs treatment caused an accumulation of intracellular ferrous iron and the onset of lipid peroxidation in DLBCL cells as well as the suppressed expression of anti-ferroptosis protein Glutathione Peroxidase 4 (GPX4), thereby leading to increased ferroptosis. Mechanistically, IONs increased cellular lipid peroxidation through the generation of ROS via the Fenton reaction and regulating the iron metabolism-related proteins, such as ferroportin (FPN) and transferrin receptor (TFR), which elevated the intracellular labile iron pool (LIP). Hence, our findings suggest the potential therapeutic effect of IONs on the treatment of patients with DLBCL.

Keywords: Diffuse large B cell lymphoma, iron oxide nanoparticles, ferroptosis, tumor growth

Introduction

Among non-Hodgkin's lymphoma, DLBCL is the most common subtype and accounts for about 30-40% of all cases worldwide according to the large population-based statistical analysis [1, 2]. The current standard R-CHOP chemotherapy (rituximab, cyclophosphamide, doxorubicin, vincristine, and prednisone) for DLBCL results in a complete recovery in approximately 50-70% of DLBCL patients; however, about one-third of the patients develop relapsed or refractory disease. Hence, it is imperative to identify novel targets and to develop effective therapies for patients with relapsed or refractory DLBCL [3, 4].

Ferumoxytol and other IONs were initially used as contrast agents and drug carriers preclinically and clinically [5-8] and were approved by the Food and Drug Administration (FDA) for treating iron deficiency anemia [9]. Recently, IONs have been reported to exert antitumor effects on hematopoietic and lymphoid tumors such as leukemia; however, the molecular mechanisms underlying the IONs' antitumor activity have not been fully elucidated [10, 11]. Structurally, Ferumoxytol is a superparamagnetic iron oxide that can be delivered into the human body where ferrous and ferric iron are released and trigger Fenton reactions in the presence of peroxides, thereby leading to the production of ROS [12, 13]. ROS is closely linked to the process of ferroptosis lipid peroxidation.

In this study, we revealed the antitumor effect of IONs and further elucidated the mechanisms by which IONs induced cell death in DLBCL.

Materials and methods

Chemicals and reagents

The following chemicals were purchased: $FeCl_3$-$6H_2O$ (97%) from Sigma, Darmstadt, Germany;

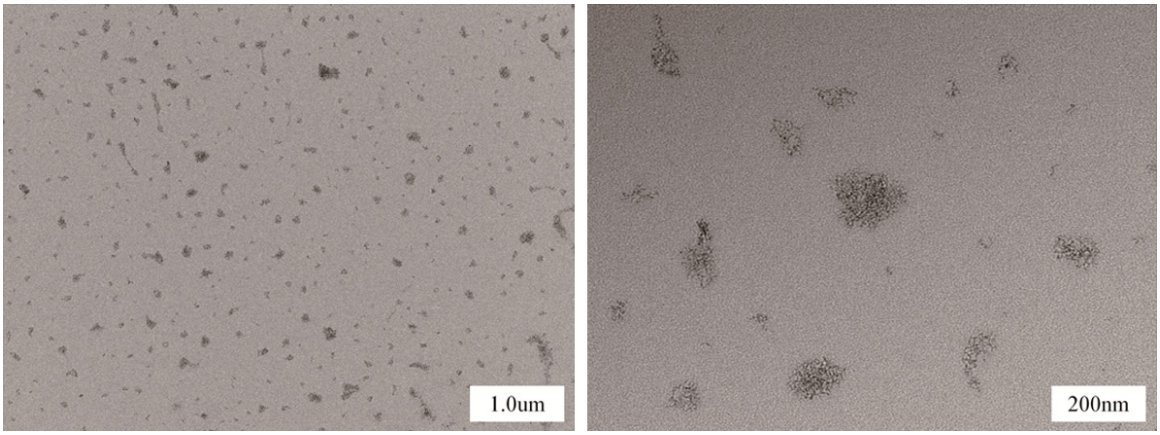

Figure 1. Transmission electron micrographs of synthetic iron oxide nanoparticles.

$FeCl_2$-$4H_2O$ (99.0%) and $FeCl_2$-$4H_2O$ (99.0%) from Aladdin, Shanghai, China; Dextran (100,000 MT) from Sangon Biotech, Shanghai, China; Ammonia from Sinopharm, Shanghai, China; FerroOrange from Dojindo, Japan; Li-perfluo from Dojindo, Japan, Penicillin/Streptomycin from Beyotime, Shanghai, China. Cell culture 1640 medium was purchased from Hyclone, Utah, USA; FBS was from Gibco, NY, USA. Cell Counting Kit-8 (CCK8) was from Beyotime, Shanghai, China. Annexin V-APC Apoptosis Assay Kit was from BestBio, Beijing, China. ECL reagent was from Pierce, Massachusetts, USA.

The following antibodies were purchased from Abcam, Cambridge, UK: anti-Glutathione Peroxidase 4 (1:2000, ab125066), anti-SLC40A1 (1:2000, ab239583), anti-Transferrin (1:1000, ab214039), anti-GPX4 antibody (1:100, ab125066), anti-SLC40A1 antibody (30 μg/ml, ab239583), and anti-Transferrin antibody (1:500, ab214039).

Anti-β-actin (1:2000) and HRP-conjugated secondary antibody (1:5000) were from ZSGB-Bio, Beijing, China.

Cell culture

Human DLBCL cell lines SUDHL-2 (activated subtype, ABC) and SUDHL-4 (germinal center subtype, GCB) were provided by Dr. Ding of The First Affiliated Hospital of USTC China and cultured in 1640 medium supplemented with 10% FBS and 1% Penicillin/Streptomycin. All cells were maintained in a 37°C humidified incubator with 5% CO_2.

Preparation of iron oxide nanoparticles

$FeCl_3$-$6H_2O$ (0.28 mol/L), $FeCl_2$-$4H_2O$ (0.14 mol/L) and Dextran (5 g) were dissolved in 25 mL of deionized water followed by the addition of 25 mL Ammonia (7.5%) under magnetic stirring. The solution was kept at 60°C for 15 min, ultrasonicated for 30 min, and then heated to 100°C for 30 min. The solution was ultrasonicated again for 30 min and filtrated through a 450 μm and a 220 μm membranes (**Figure 1**).

Proliferation assays

Cell proliferation was assessed by CCK8 assay. Briefly, SUDHL-2 and SUDHL-4 cells (3×10^4 cells/100 μL) were seeded in 96-well plates and treated with different concentrations of IONs (0, 300, 600, and 1200 ug/ml). Cells in control group were treated with different concentrations of dextran (0, 300, 600, and 1200 ug/ml). After treatment for 72 hours, 10 μL of the CCK8 solution was added to each well for 2 hours, and the optical density (OD) values at 450 nm was measured by a plate reader. The results represented the average readings of five wells.

Apoptosis analysis

Cell apoptosis was analyzed by using Annexin V-APC Assay Kit following the manufacturer's protocol. Briefly, SUDHL-2 and SUDHL-4 cells were treated with IONs (1200 ug/ml) for 48 hours, and the cell pellets were collected. After washing with PBS, the cells were stained in Annexin V-APC and propidium iodide (PI) staining solution at 4°C for 30 minutes in dark and

analyzed by FACS (BD FACScelesta3, San Jose, CA, USA).

ROS measurement

The intracellular ROS level was evaluated by the uptake of DCFH-DA (Fluorescent Probes, BestBio, Beijing, China). To visualize the ROS production, 5 × 10^5 SUDHL-2 and SUDHL-4 cells were seeded in 6-well plates and treated with IONs (1200 ug/ml) for 48 hours, while the control group was treated with vehicle PBS. Then, the cells were washed once with PBS and stained with DCFH-DA (1:2000) for 30 minutes at 37°C in dark. Cells were resuspended in PBS, and green fluorescence was detected by FACS analysis. Data were collected from at least 10,000 cells. The fluorescent intensity of each group was normalized to that of the control group.

Fe^{2+} detection

To detect intracellular Fe^{2+}, FerroOrange was used according to the manufacturer's instruction. Briefly, SUDHL-2 and SUDHL-4 cells were treated with IONs (1200 ug/ml) for 48 hours and stained with 1 μmol/L FerroOrange for 30 minutes at 37°C, while cells in control group were treated with PBS. Images were acquired using a Leica SP5 confocal laser scanning microscope (Leica Microsystems) equipped with a Plan Apochromat 60 × 1.40 NA oil immersion objective. Analysis of Fe^{2+} in SUDHL-2 and SUDHL-4 cells was performed by measuring the intensity of fluorescence of from at least 100 cells for each treatment condition. Fluorescence intensity was determined by Image J (National Institutes of Health).

Lipid peroxides measurement

To visualize the lipid ROS, cells were seeded in 6-well plates, treated with IONs for 48 hours, and stained with 10 μmol/L Liperfluo for 30 minutes at 37°C in dark. The cells were then washed twice with PBS and observed by a Leica SP5 confocal laser scanning microscope (Leica Microsystems) equipped with a Plan Apochromat 60 × 1.40 NA oil immersion objective. Fluorescence intensity was determined by Image J.

Western blot analysis

Western blot analysis was carried out using standard protocol. Briefly, cells were lysed in RIPA buffer containing protease inhibitors, and the cell lysates were obtained by centrifugation followed by protein quantification using BCA. Approximately 20 μg proteins were separated by SDS-PAGE, transferred to polyvinylidene difluoride (PVDF) membranes, and blocked with 5% skim milk in TBST at room temperature for 1 hour, followed by incubation in the indicated primary antibodies at 4°C overnight. After extensive washing with TBST, the membranes were incubated with HRP-conjugated secondary antibody for 1 hour at room temperature, and the proteins were visualized using ECL reagent with a chemiluminescence imaging instrument (Tanon5200, Shanghai, China). Protein expression was quantified using ImageJ software and normalized to β-actin.

Xenagraft tumor model

BALB/C female nude mice (age of 4-5 weeks, 16-20 g) were obtained from GemPharmatech Co., Ltd. (Nanjing, China). Mice were fed with standard rodent chow and water ad libitum and were housed in a specific pathogen-free (SPF) facility under controlled temperature and humidity at the School of Basic Medical Sciences, Anhui Medical University. All experiments using animals were approved by the Animal Ethics Committee of Anhui Medical University. After a week of acclimatization, 2 × 10^7 SUDHL-4 cells in 200 ul of PBS were subcutaneously injected into the right axillary regions of the mice. Tumor growth was monitored every two days, and the tumor volume was calculated using formula: (length × width × width)/2. When the tumor volume reached approximately 100 mm^3, the mice were randomly divided into four groups: the 3 mg/kg IONs IV (Intravenous injection) group (n=5), the 6 mg/kg IONs IV (Intravenous injection) group (n=6), the 6 mg/kg IONs IP (Intraperitoneal injection) group (n=5), and the control group injected with PBS (n=5). Mice in each group received injection every other day for 12 days (the first day of administration was recorded as day 0), and the weight and tumor size of each mouse were recorded every other day. When the tumor volume reached approximately 2000 mm^3, mice were euthanized, and the tumors were extracted for further analysis.

Transmission electron microscopy (TEM)

Standard protocol for sample preparation was followed. Briefly, 1 mm^3 of fresh tumor tissue

was fixed in 2.5% glutaraldehyde overnight at 4°C, embedded, and cut into 60-80 nm ultrathin sections. The sections were then subjected to uranium and lead double staining. Mitochondrial structure was studied under TEM, and the images at different magnifications (× 10000 and × 25000) were captured.

Immunohistochemistry (IHC) staining

Standard IHC staining protocol was followed. Briefly, subcutaneous tumor specimens were fixed in 4% formalin, embedded in paraffin, and cut into 3 μm sections. All sections were dewaxed in xylene, rehydrated, and antigen retrieved with sodium citrate solution (pH=6), except for anti-Transferrin antibody where Tris/EDTA buffer (pH=9) was used. After blocking in goat serum, sections were incubated with primary antibodies overnight at 4°C, followed by treatment with 3% hydrogen peroxide to block the endogenous peroxidase activity. For DAB staining, the sections were incubated with biotinylated secondary antibodies for 20 minutes and counter stained with hematoxylin. Images of several random fields in each section were captured under different magnifications (× 200 and × 400) using an Olympus BX51TF microscope (Olympus, Tokyo, Japan), and the signals were analyzed by two professional pathologists.

Statistical analysis

All data were presented as the mean ± SEM from three independent experiments. The two-tailed Student's T-test and one-way ANOVA of GraphPadPrism (version 8.0.2) were used to determine statistical significance. The statistical calculations were conducted using SPSS software (version 25). A value of $P<0.05$ was considered statistically significant.

Results

IONs inhibited cell proliferation while induced apoptosis in DLBCL

To explore the effects of IONs in DLBCL cells, we first examined the proliferation of SUDHL-2 and SUDHL-4 cells upon IONs or dextran treatment for 48 hours. CCK-8 assays showed that IONs decreased DLBCL cell viability in a dose-dependent manner, while control dextran had no effect (**Figure 2A-C**). In contrast, IONs induced the apoptosis of DLBCL cells, as measured by flow cytometry with Annexin V-APC/PI staining (**Figure 2D**), indicating that IONs treatment caused cell death in DLBCL.

Ferroptosis contributed to IONs-induced cell death in DLBCL

Other studies have reported that IONs induce the ROS level. Hence, in our study, we verified this effect by measuring the production of total ROS under IONs treatment. The flow cytometric analysis results indicated that, compared to PBS treatment, IONs treatment significantly increased the ROS level in SUDHL-2 and SUDHL-4 cells (**Figure 3A**). In addition, we measured the level of intracellular Fe^{2+} after IONs treatment in DLBCL cells to further demonstrate the effect of IONs on intracellular iron metabolism. As shown in **Figure 3B**, IONs treatment induced excessive iron content in SUDHL-2 and SUDHL-4 cells as indicated by higher FerroOrange signals compared to control cells. Furthermore, we detected lipid peroxidation in SUDHL-2 and SUDHL-4 cells by Liperfluo staining. As shown in **Figure 3C**, Liperfluo signal was significantly increased in IONs-treated cells, indicating that IONs induced lipid peroxidation in DLBCL cells. Similarly, the expression of TFR was significantly increased after IONs treatment. Since ROS production level is closely related to ferroptosis, as ferroptosis is mainly dependent on the intracellular iron accumulation and lipid peroxidation, our data suggested that ferroptosis was induced by IONs treatment. In support with this, the expression of ferroptosis negative regulators such as GPX4 and SLC40A1 was significantly decreased after IONs treatment (**Figure 3D**).

IONs inhibited the growth of xenograft tumor

After having observed the growth-inhibitory effect of IONs in DLBCL cells in vitro, we used mouse xenograft tumor model to explore whether IONs could inhibit tumor growth in vivo. SUDHL-4 cells-derived subcutaneous tumors were apparent 10 days after cell implant. Then, the mice were randomly divided into four groups and treated with different concentration of IONs via IV or IP. Mice in control group received PBS injection. We found that IV injection of 3 mg/kg or 6 mg/kg IONs significantly inhibited tumor growth exhibiting reduced tumor size and weight, compared to the tumor growth in IP injected or control group mice. There was no significant difference between

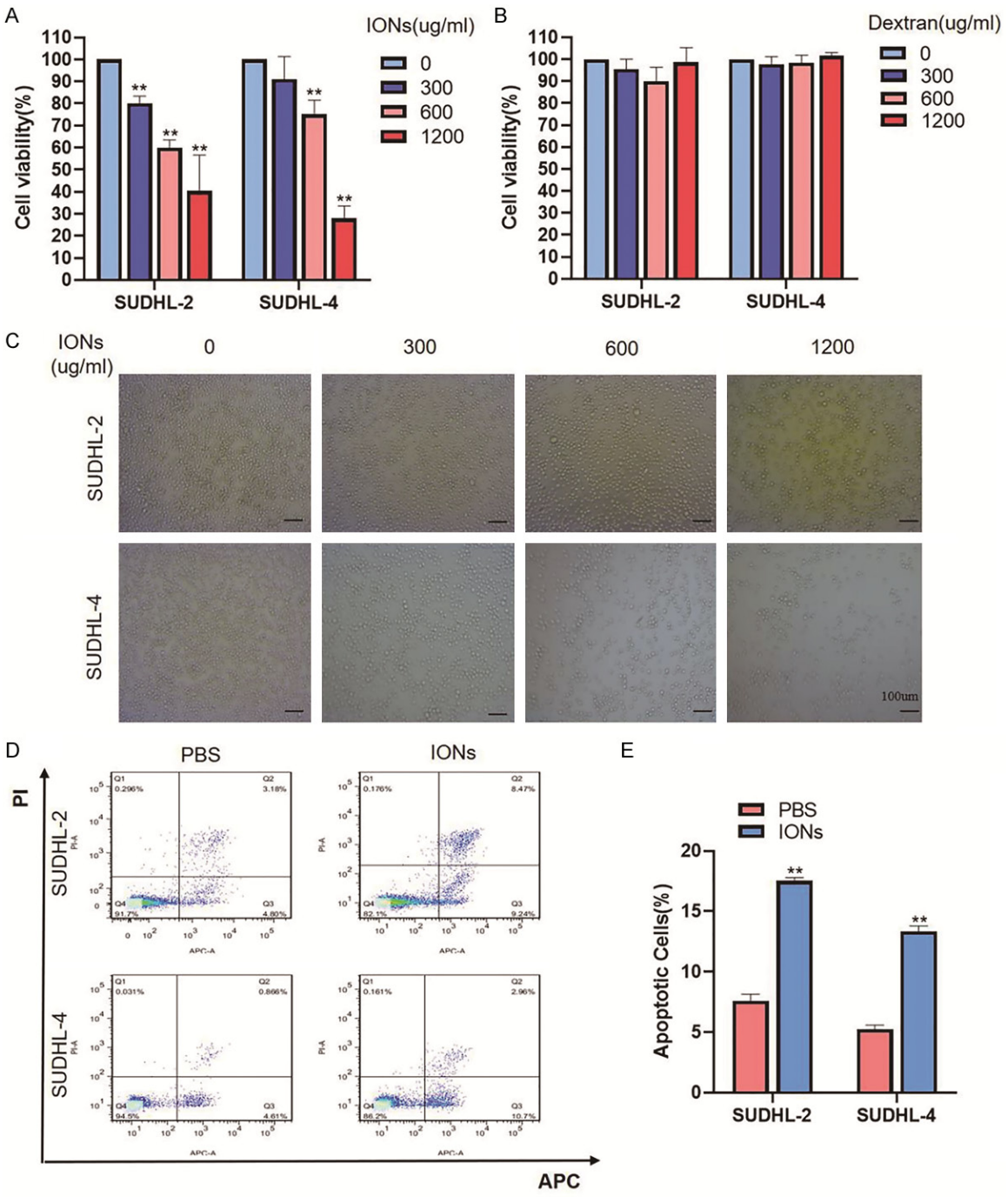

Figure 2. IONs inhibit cell proliferation and induce apoptosis in DLBCL cells. The viability of DLBCL cells after treatment with increasing concentrations of IONs (A) and Dextran (B) for 72 h. ** P<0.01, compared to untreated cells; (C) Representative cell morphological changes were detected under a microscope after treatment with IONs for 72 h. (D, E) Representative results of annexin V/APC/PI staining and quantitative analysis. ** *P*<0.01.

different doses of IONs, nor between IV or IP injection (**Figure 4B**, **4C**). The carcass weight among all mice was similar (**Figure 4D**), indicating the difference in tumor growth was not caused by mouse bodyweight.

IONs induced ferroptosis in vivo.

Furthermore, the ultrastructure of the tumor tissues in IONs-treated or vehicle-treated groups was examined by transmission electron

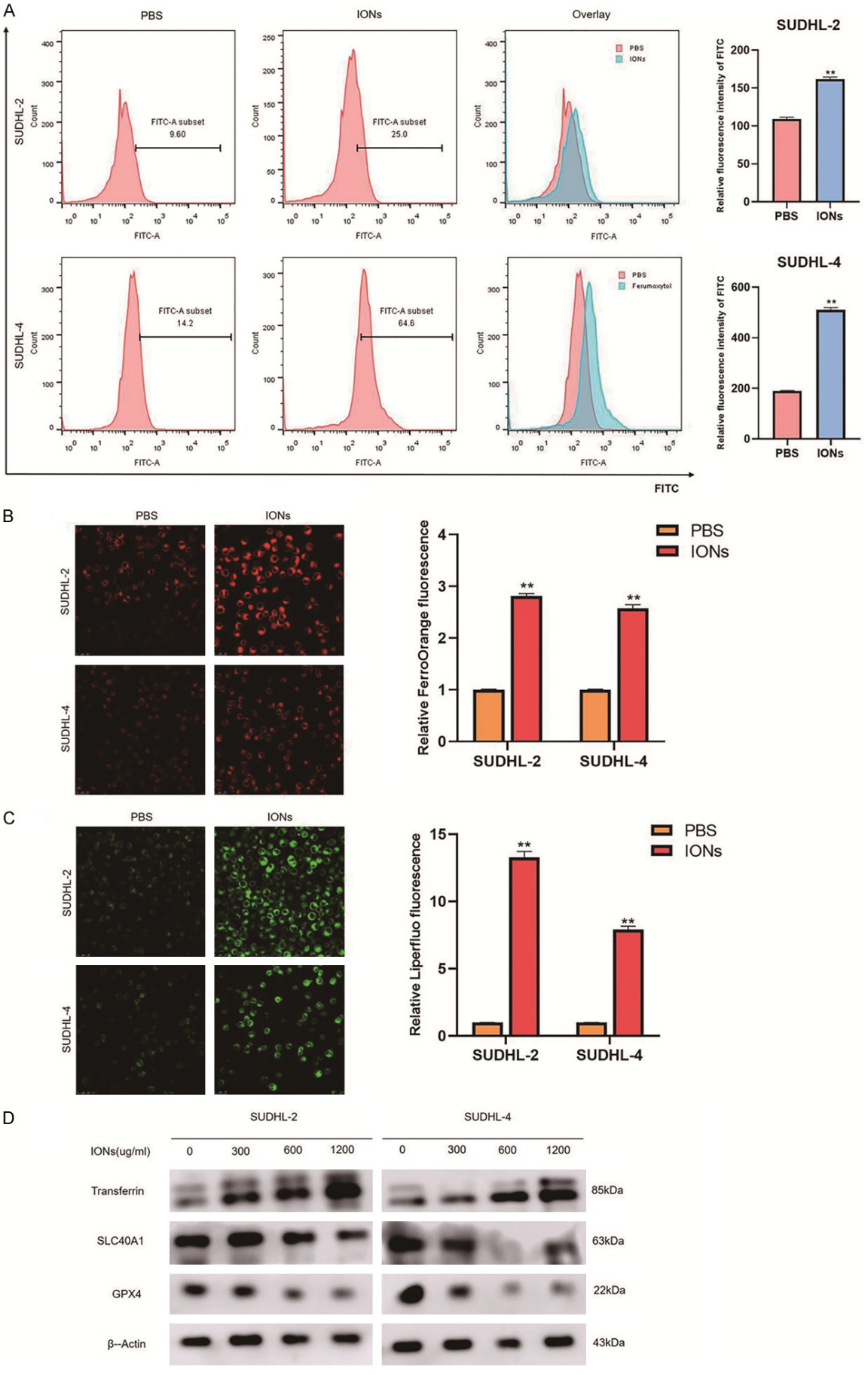
A
PBS
IONs
Overlay
SUDHL-2
SUDHL-4
FITC-A subset 9.60
FITC-A subset 25.0
FITC-A subset 14.2
FITC-A subset 64.6
Count
FITC-A
PBS
IONs
Ferumoxytol
FITC
SUDHL-2
SUDHL-4
Relative fluorescence intensity of FITC
PBS
IONs
B
PBS
IONs
SUDHL-2
SUDHL-4
Relative FerroOrange fluorescence
C
Relative Liperfluo fluorescence
D
SUDHL-2
SUDHL-4
IONs(ug/ml)
0
300
600
1200
Transferrin
SLC40A1
GPX4
β--Actin
85kDa
63kDa
22kDa
43kDa

Figure 3. Ferroptosis contributes to IONs-induced cell death in DLBCL cells. A. The cellular ROS level was analyzed by using flow cytometer; B. Intracellular Fe^{2+} in SUDHL-2 and SUDHL-4 cells after IONs treatment was determined by FerroOrange. Scale bar: 25 μm; C. Lipid peroxidation in SUDHL-2 and SUDHL-4 cells was detected by Liperfluo after IONs treatment. Scale bar: 25 μm; D. The expression of several key ferroptosis regulators in DLBCL cells after IONs treatment was examined by western blot analysis. ** P<0.01.

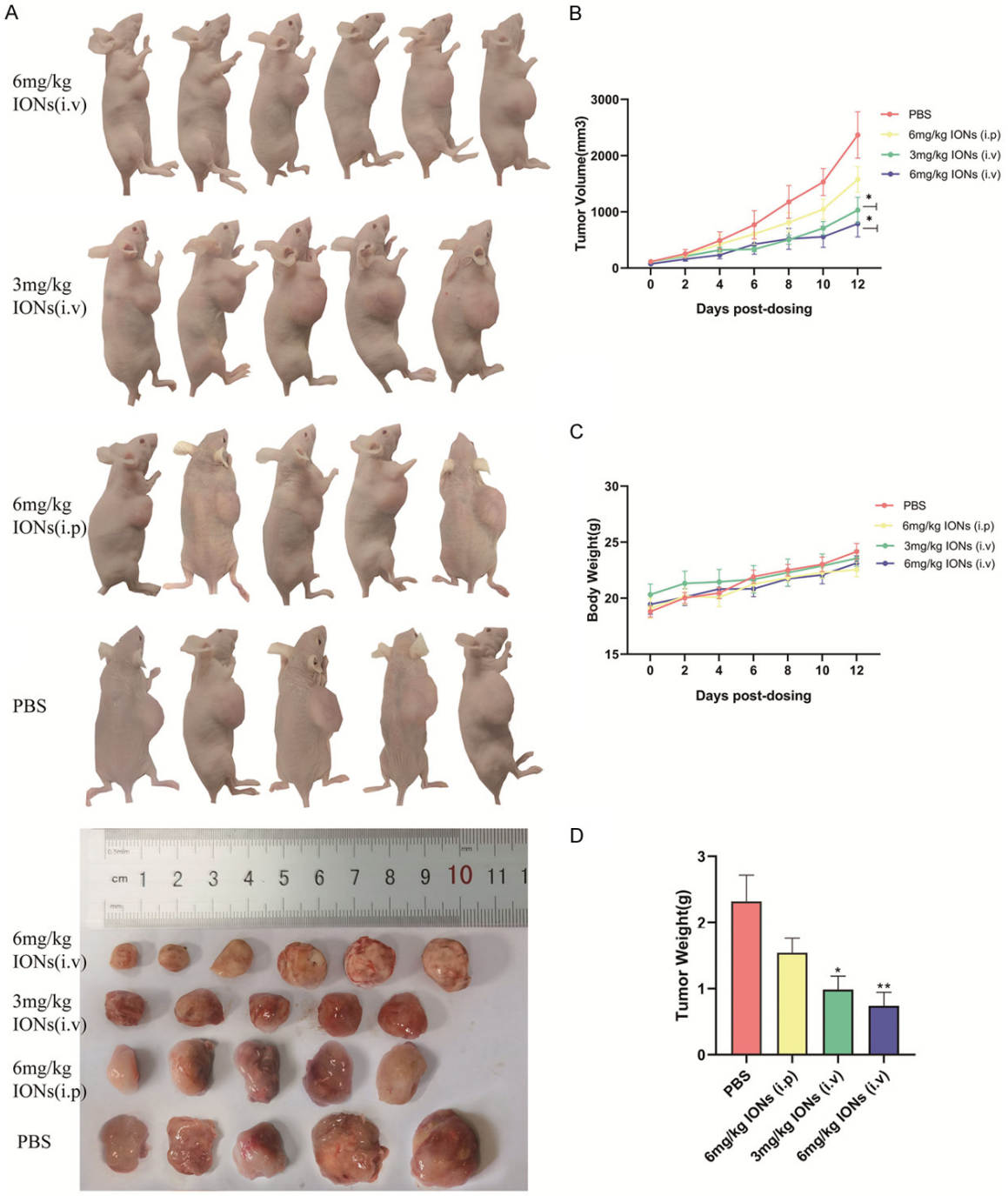

Figure 4. IONs inhibit the growth of xenograft tumor. 2 × 10^7 SUDHL-4 cells were subcutaneously injected into the right sides of nude mice. When tumor volume reached about 100 mm^3, mice were randomly divided into four groups and received IONs (3 mg/kg or 6 mg/kg) or PBS via IV or IP as indicated every other day. A. Representative images of mice from these four groups and their subcutaneous tumors dissected after euthanasia. B. The tumor volume in mice from these four groups. Subcutaneous tumor volume was reduced in two groups, 3 mg/kg IONs IV (n=5) and 6 mg/kg IONs IV (n=6). No statistical difference in tumor volume between these two groups. C. The mice weight

of four groups. D. The subcutaneous tumor weights of four groups. Tumor weight in 3 mg/kg IONs IV- and 6 mg/kg IONs IV-injected groups was statistically different from the control group but not statistically different between these two groups.

microscopy. The results revealed that, compared to the control group, 6 mg/kg IONs IV injection resulted in significant ferroptosis-associated mitochondrial structure changes, such as increased membrane density, reduced mitochondrial volume, and decreased or absent mitochondrial cristae (**Figure 5A**). Consistently, IHC staining showed that the expression of ferroptosis negative regulators GPX4 and FPN was significantly decreased in the tumor of 6 mg/kg IONs IV treated mice, while the expression of TFR which is associated with intracellular iron accumulation was increased (**Figure 5B**). Collectively, these results demonstrated that IONs could also induce ferroptosis in vivo and inhibited the growth of xenograft tumor.

Discussion

Iron oxide nanoparticles are used as drug carriers and contrast agents in a variety of tumors for early diagnosis, adjuvant therapy, and prognosis prediction [16-19], and their dextran-coated compound ferumoxytol has shown direct anti-tumor effects [10, 11]. Many studies have demonstrated that iron oxide nanoparticles can inhibit tumor growth and migration by polarizing tumor-associated macrophages into M1 cells [20-23] and promote apoptosis by assisting in the induction of ferroptosis through the Fenton response [24, 25]. It is also exciting to note that a novel iron oxide nanoparticles coated with gallic acid and polyacrylic acid (IONP-GA/PAA) possess intrinsic cytotoxic activity on various cancer cell lines by inducing ferroptosis in vitro [26]. In this study, we were the first to demonstrate the ability of ferumoxytol, another novel iron oxide nanoparticles with dextran coating, to induce ferroptosis and inhibit DLBCL growth in vitro and in vivo and identify an additional pathway for iron oxide nanoparticles to induce ferroptosis in addition to the conventional Fenton reaction.

We found that IONs significantly inhibited the proliferation and induced the apoptosis of DLBCL cells in vitro, which was not caused by the activity of dextran coating. Xenograft tumor growth in mice further confirmed the growth inhibitory effect of IONs. Nevertheless, the efficacy of IONs did not show the same dose correlation as in vitro, as no statistical difference between the 3 mg/kg IONs and 6 mg/kg IONs groups on tumor growth was observed, which was consistent with the findings on tumor progression in breast cancer [11] and was presumably related to the absorption threshold of IONs in vivo. Furthermore, in our study, we observed the efficacy of IONs was different with different mode of injection, as intraperitoneal injection of IONs didn't inhibit DLBCL tumor growth, contradicting to the findings in breast cancer. We hypothesized that, although DLBCL is a solid tumor like breast cancer, it is still part of the hematopoietic and lymphoid tumors. Tail vein administration is more direct and consistent with the routine administration of IONs in clinical practice [27].

Ferroptosis, a novel form of regulated cell death, has been studied in a variety of tumors since its discovery and has been contributed to the antitumor effects of several drugs [28]. In DLBCL, ferroptosis-related genes were found to be associated with prognosis [29, 30]. Our study further demonstrated the functional role of ferroptosis in DLBCL. It has been well known that intracellular iron accumulation and lipid peroxidation are two key aspects of ferroptosis [31, 32], and that the accumulation of ROS and the occurrence of lipid peroxidation are closely related [31, 32]. We revealed that IONs induced lipid peroxidation in DLBCL cells by accumulating ROS through the Fenton reaction in vitro, and that the expression of the ferroptosis negative regulator GPX4 was reduced, with was further validated with mouse xenograft tumors. Moreover, we showed that IONs could cause abnormal expression of proteins related to iron metabolism. IONs reduced the expression of FPN which decreased intracellular iron efflux, while increased the expression of TFR which enhanced extracellular iron input. Through these two synergistic effects, IONs increased the labile iron pool, thus contributing to ferroptosis.

From a clinical perspective, because the main component of IONs is elemental iron which is already present in the body and is closely regulated, IONs have fewer side effects and no

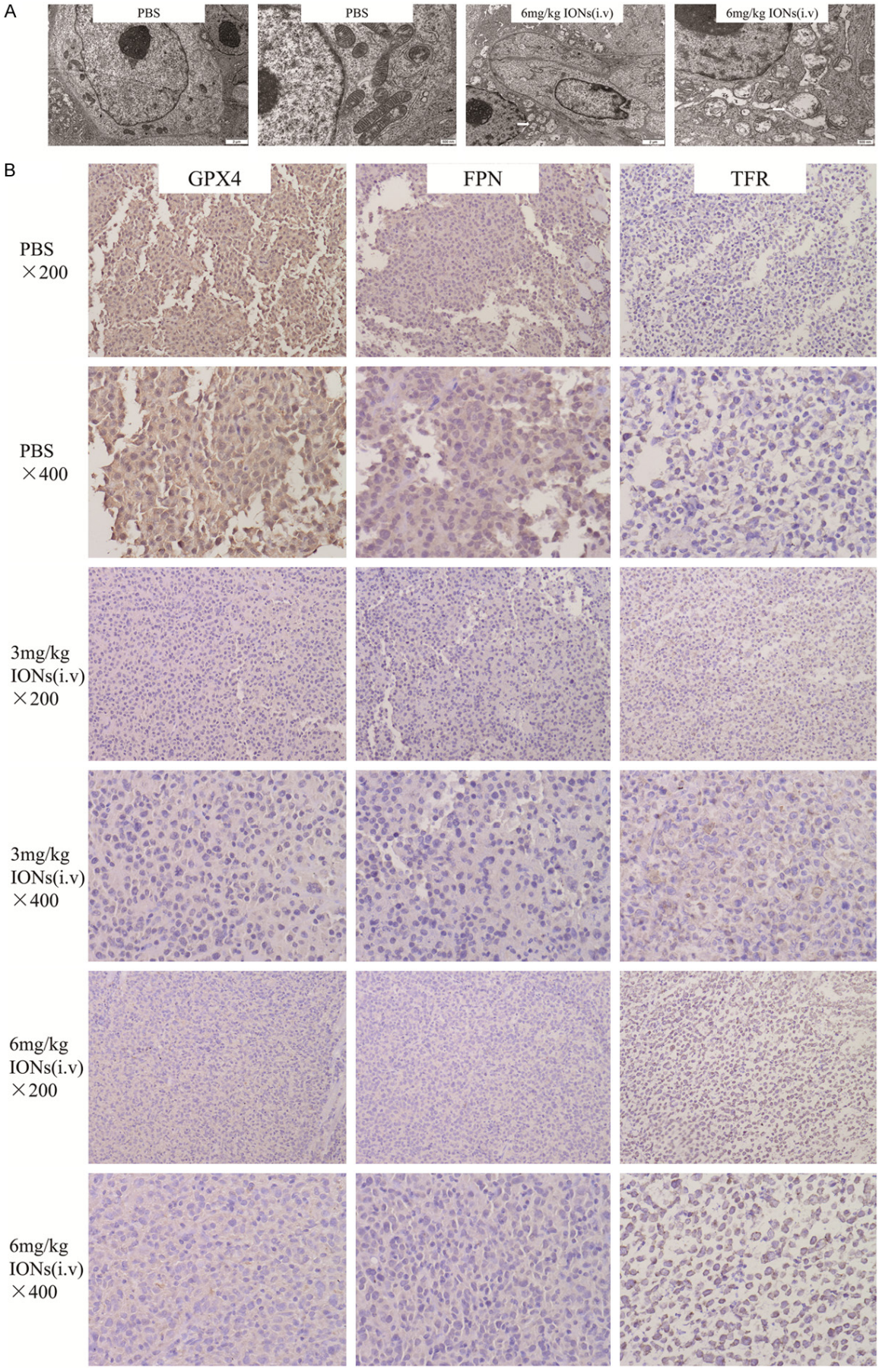
A
PBS
PBS
6mg/kg IONs(i.v)
6mg/kg IONs(i.v)
B
GPX4
FPN
TFR
PBS ×200
PBS ×400
3mg/kg IONs(i.v) ×200
3mg/kg IONs(i.v) ×400
6mg/kg IONs(i.v) ×200
6mg/kg IONs(i.v) ×400

Figure 5. IONs induce ferroptosis in vivo. A. Electron microscopy analysis of DLBCL cells treated with vehicle or IONs (6 mg/kg, IV). The white arrowhead indicated a mitochondrion with membrane rupture and reduced cristae. B. Immunohistochemistry staining of GPX4, FPN, and TFR were performed on SUDHL-4-derived tumors after intravenous IONs treatment at different doses. Scale bar: 50 μm; original magnification × 200 and × 400.

acute hematological and non-hematological toxicities which are associated with drugs in standard chemotherapy regimens. The main side effect of FDA-approved IONs drug is iron overload [33].

In summary, our study highlighted the promising application of IONs in the treatment of patients with DLBCL and provided new therapeutic strategies targeting ferroptosis in the future.

Acknowledgements

We are grateful to Pro. Lu from Hefei University of Technology and Dr. Dong from University of Science and Technology of China for the preparation of iron oxide nanoparticles. We are also thankful to Dr. Ding from The First Affiliated Hospital of USTC for providing the DLBCL cell lines. The authors thank P2 Laboratory Animal Research, College of Basic Medical Sciences, for the excellent animal care. The animal experiments were approved by the Animal Ethics Committee of Anhui Medical University. This work was supported by National Natural Science Foundation of China (81700194), College Natural Science Foundation of Anhui Province (KJ2021A0214).

Disclosure of conflict of interest

None.

Address correspondence to: Yan-Li Li, Department of Pathology, School of Basic Medical Sciences, Anhui Medical University, Hefei 230032, Anhui, China; Department of Pathology, The Second Affiliated Hospital of Anhui Medical University, Hefei 230601, Anhui, China. E-mail: liyanli_rainbow126@163.com

References

[1] Chihara T, Wada N, Ikeda J, Fujita S, Hori Y, Ogawa H, Sugiyama H, Nomura S, Matsumura I, Hino M, Kanakura Y, Morii E and Aozasa K. Frequency of intravascular large B-cell lymphoma in Japan: study of the Osaka Lymphoma Study Group. J Hematol Oncol 2011; 4: 14.

[2] Swerdlow SH, Campo E, Pileri SA, Harris NL, Stein H, Siebert R, Advani R, Ghielmini M, Salles GA, Zelenetz AD and Jaffe ES. The 2016 revision of the World Health Organization classification of lymphoid neoplasms. Blood 2016; 127: 2375-2390.

[3] Camicia R, Winkler HC and Hassa PO. Novel drug targets for personalized precision medicine in relapsed/refractory diffuse large B-cell lymphoma: a comprehensive review. Mol Cancer 2015; 14: 207.

[4] Feugier P, Van Hoof A, Sebban C, Solal-Celigny P, Bouabdallah R, Fermé C, Christian B, Lepage E, Tilly H, Morschhauser F, Gaulard P, Salles G, Bosly A, Gisselbrecht C, Reyes F and Coiffier B. Long-term results of the R-CHOP study in the treatment of elderly patients with diffuse large B-cell lymphoma: a study by the Groupe d'Etude des Lymphomes de l'Adulte. J Clin Oncol 2005; 23: 4117-26.

[5] Ansari C, Tikhomirov GA, Hong SH, Falconer RA, Loadman PM, Gill JH, Castaneda R, Hazard FK, Tong L, Lenkov OD, Felsher DW, Rao J and Daldrup-Link HE. Development of novel tumor-targeted theranostic nanoparticles activated by membrane-type matrix metalloproteinases for combined cancer magnetic resonance imaging and therapy. Small 2014; 10: 566-75, 417.

[6] Corot C, Robert P, Idée JM and Port M. Recent advances in iron oxide nanocrystal technology for medical imaging. Adv Drug Deliv Rev 2006; 58: 1471-504.

[7] Neuwelt EA, Várallyay CG, Manninger S, Solymosi D, Haluska M, Hunt MA, Nesbit G, Stevens A, Jerosch-Herold M, Jacobs PM and Hoffman JM. The potential of ferumoxytol nanoparticle magnetic resonance imaging, perfusion, and angiography in central nervous system malignancy: a pilot study. Neurosurgery 2007; 60: 601-11; discussion 611-2.

[8] Ruan Y, Xiong Y, Fang W, Yu Q, Mai Y, Cao Z, Wang K, Lei M, Xu J, Liu Y, Zhang X, Liao W and Liu J. Highly sensitive Curcumin-conjugated nanotheranostic platform for detecting amyloid-beta plaques by magnetic resonance imaging and reversing cognitive deficits of Alzheimer's disease via NLRP3-inhibition. J Nanobiotechnology 2022; 20: 322.

[9] Lu M, Cohen MH, Rieves D and Pazdur R. FDA report: ferumoxytol for intravenous iron therapy in adult patients with chronic kidney disease. Am J Hemato 2010; 85: 315-9.

[10] Trujillo-Alonso V, Pratt EC, Zong H, Lara-Martinez A, Kaittanis C, Rabie MO, Longo V, Becker MW, Roboz GJ, Grimm J and Guzman ML. FDA-approved ferumoxytol displays anti-

leukaemia efficacy against cells with low ferroportin levels. Nat Nanotechnol 2019; 14: 616-622.
[11] Zanganeh S, Hutter G, Spitler R, Lenkov O, Mahmoudi M, Shaw A, Pajarinen JS, Nejadnik H, Goodman S, Moseley M, Coussens LM and Daldrup-Link HE. Iron oxide nanoparticles inhibit tumour growth by inducing pro-inflammatory macrophage polarization in tumour tissues. Nat Nanotechnol 2016; 11: 986-994.
[12] Birben E, Sahiner UM, Sackesen C, Erzurum S and Kalayci O. Oxidative stress and antioxidant defense. World Allergy Organ J 2012; 5: 9-19.
[13] Gao L, Zhuang J, Nie L, Zhang J, Zhang Y, Gu N, Wang T, Feng J, Yang D, Perrett S and Yan X. Intrinsic peroxidase-like activity of ferromagnetic nanoparticles. Nat Nanotechnol 2007; 2: 577-583.
[14] Dixon SJ, Lemberg KM, Lamprecht MR, Skouta R, Zaitsev EM, Gleason CE, Patel DN, Bauer AJ, Cantley AM, Yang WS, Morrison B 3rd and Stockwell BR. Ferroptosis: an iron-dependent form of nonapoptotic cell death. Cell 2012; 149: 1060-1072.
[15] Lin MT and Beal MF. Mitochondrial dysfunction and oxidative stress in neurodegenerative diseases. Nature 2006; 443: 787-95.
[16] Liolios C, Koutsikou TS, Salvanou EA, Kapiris F, Machairas E, Stampolaki M, Kolocouris A, Efthimiadou EK and Bouziotis P. Synthesis and in vitro proof-of-concept studies on bispecific iron oxide magnetic nanoparticles targeting PSMA and GRP receptors for PET/MR imaging of prostate cancer. Int J Pharm 2022; 624: 122008.
[17] Dadfar SM, Roemhild K, Drude NI, von Stillfried S, Knüchel R, Kiessling F and Lammers T. Iron oxide nanoparticles: diagnostic, therapeutic and theranostic applications. Adv Drug Deliv Rev 2019; 138: 302-325.
[18] Mohammed L, Gomaa HG, Ragab D and Zhu J. Magnetic nanoparticles for environmental and biomedical applications: a review. Particuology 2017; 30: 1-14.
[19] Kader A, Kaufmann JO, Mangarova DB, Moeckel J, Brangsch J, Adams LC, Zhao J, Reimann C, Saatz J, Traub H, Buchholz R, Karst U, Hamm B and Makowski MR. Iron oxide nanoparticles for visualization of prostate cancer in MRI. Cancers (Basel) 2022; 14: 2909.
[20] Liu X, Xu Y, Li Y, Pan Y, Zhao S and Hou Y. Ferumoxytol-β-glucan inhibits melanoma growth via interacting with dectin-1 to polarize macrophages into M1 phenotype. Int J Med Sci 2021; 18: 3125-3139.
[21] Zhang W, Cao S, Liang S, Tan CH, Luo B, Xu X and Saw PE. Differently charged super-paramagnetic iron oxide nanoparticles preferentially induced M1-like phenotype of macrophages. Front Bioeng Biotechnol 2020; 8: 537.
[22] Wang G, Zhao J, Zhang M, Wang Q, Chen B, Hou Y and Lu K. Ferumoxytol and CpG oligodeoxynucleotide 2395 synergistically enhance antitumor activity of macrophages against NSCLC with EGFRL858R/T790M mutation. Int J Nanomedicine 2019; 14: 4503-4515.
[23] Zhao J, Zhang Z, Xue Y, Wang G, Cheng Y, Pan Y, Zhao S and Hou Y. Anti-tumor macrophages activated by ferumoxytol combined or surface-functionalized with the TLR3 agonist poly (I:C) promote melanoma regression. Theranostics 2018; 8: 6307-6321.
[24] Li Q, Su R, Bao X, Cao K, Du Y, Wang N, Wang J, Xing F, Yan F, Huang K and Feng S. Glycyrrhetinic acid nanoparticles combined with ferrotherapy for improved cancer immunotherapy. Acta Biomater 2022; 144: 109-120.
[25] Zhang Y, Fu X, Jia J, Wikerholmen T, Xi K, Kong Y, Wang J, Chen H, Ma Y, Li Z, Wang C, Qi Q, Thorsen F, Wang J, Cui J, Li X and Ni S. Glioblastoma therapy using codelivery of cisplatin and glutathione peroxidase targeting siRNA from iron oxide nanoparticles. ACS Appl Mater Interfaces 2020; 12: 43408-43421.
[26] Fernández-Acosta R, Iriarte-Mesa C, Alvarez-Alminaque D, Hassannia B, Wiernicki B, Díaz-García AM, Vandenabeele P, Vanden Berghe T and Pardo Andreu GL. Novel iron oxide nanoparticles induce ferroptosis in a panel of cancer cell lines. Molecules 2022; 27: 3970.
[27] Huang Y, Hsu JC, Koo H and Cormode DP. Repurposing ferumoxytol: diagnostic and therapeutic applications of an FDA-approved nanoparticle. Theranostics 2022; 12: 796-816.
[28] Su Y, Zhao B, Zhou L, Zhang Z, Shen Y, Lv H, AlQudsy LHH and Shang P. Ferroptosis, a novel pharmacological mechanism of anti-cancer drugs. Cancer Lett 2020; 483: 127-136.
[29] Chen H, He Y, Pan T, Zeng R, Li Y, Chen S, Li Y, Xiao L and Zhou H. Ferroptosis-related gene signature: a new method for personalized risk assessment in patients with diffuse large B-cell lymphoma. Pharmgenomics Pers Med 2021; 14: 609-619.
[30] Xiong D, Li M and Zeng C. Construction and validation of a risk scoring model for diffuse large B-cell lymphoma based on ferroptosis-related genes and its association with immune infiltration. Transl Oncol 2022; 16: 101314.
[31] Shen Z, Song J, Yung BC, Zhou Z, Wu A and Chen X. Emerging strategies of cancer therapy based on ferroptosis. Adv Mater 2018; 30: e1704007.
[32] Hassannia B, Vandenabeele P and Vanden Berghe T. Targeting ferroptosis to iron out cancer. Cancer Cell 2019; 35: 830-849.
[33] Rosner MH and Auerbach M. Ferumoxytol for the treatment of iron deficiency. Expert Rev Hematol 2011; 4: 399-406.